International Journal of Gravitation and Theoretical Physics
https://www.sciltp.com/journals/ijgtp

Article

Stability Ranges of Magnetic Black Holes and Mirror (Topological) Stars in 5D Gravity

Kirill A. Bronnikov [1,2,3], Sergei V. Bolokhov [2,*] and Milena V. Skvortsova [2]

[1] Center of Gravitation and Fundamental Metrology, Rostest, Ozyornaya ul. 46, Moscow 119361, Russia
[2] Institute of Gravitation and Cosmology, RUDN University, ul. Miklukho-Maklaya 6, Moscow 117198, Russia
[3] National Research Nuclear University "MEPhI", Kashirskoe sh. 31, Moscow 115409, Russia
* Correspondence: bolokhov-sv@rudn.ru

How To Cite: Bronnikov, K.A.; Bolokhov, S.V.; Skvortsova, M.V. Stability Ranges of Magnetic Black Holes and Mirror (Topological) Stars in 5D Gravity. *International Journal of Gravitation and Theoretical Physics* **2026**, *2*(1), 2. https://doi.org/10.53941/ijgtp.2026.100002

Received: 2 November 2025
Revised: 12 February 2026
Accepted: 17 February 2026
Published: 12 March 2026

Abstract: We discuss static, spherically symmetric solutions to the 5D Einstein-Maxwell equations (belonging to wide classes of multidimensional solutions known at least from the 1990s) and select among them those which must observationally look like local objects whose surface reflects back particles or signals getting there, the so-called mirror stars (also called "topological stars" by some authors). Their significant parameters are the Schwarzschild mass m and the magnetic charge q, such that $q^2 > 3m^2$, while the radius of their mirror surface is $r_b = 2q^2/(3m) > 2m$. We also discuss their black hole counterparts for which $q^2 \leq 3m^2$. For both these objects, we study spherically symmetric time-dependent perturbations and determine the stability regions in their parameter spaces. Thus, mirror stars turn out to be stable only at $r_b < r_b^{\rm crit} \approx 4.004\, m$, while the black holes prove to be stable in the whole range of their parameters. We calculate the fundamental frequencies and decay rates of black hole perturbations using the WKB and time domain methods. Our stability results disagree with some of those previously announced in the literature.

Keywords: extra dimensions; black holes; compact objects; stability

1. Introduction

Multidimensional gravity contains a great variety of possible space-time configurations, both evidently imaginary and potentially realistic ones, both in the cosmological context and in modeling compact objects with strong gravitational fields. Besides a rich collection of black hole models (see, e.g., [1–5] for reviews), there are multidimensional models of wormholes [6–10], boson stars [11–13], gravastars [14, 15], etc. that possess many features of interest but are still extensions of certain known 4D objects.

Unlike that, in the present paper we would like to discuss such hypothetic objects whose very existence becomes possible due to extra dimensions. They are still related to multidimensional black hole solutions in the following way: consider such a black hole metric and mutually substitute one of the extra coordinates and the original time coordinate [16, 17]. Such a replacement surely leads to a new solution since for the equations it does not matter which of the coordinates is interpreted as time and which is regarded "extra." It can be inferred that such solutions are almost as numerous as are black hole ones: for their existence, it is only required that among the extra dimensions there is a suitable 1D subspace. As argued in [16, 17], if this extra 1D subspace is compact and sufficiently small to be invisible by modern instruments, then the surface that had been an event horizon in the original black hole solution, now becomes a perfectly reflecting surface. We therefore proposed to call such objects *mirror stars* [18].

Various reflection phenomena in astrophysics are rather actively discussed in the literature. Different kinds of echoes have been predicted in black hole and wormhole space-times [19–22]. In particular, the authors of [23] have obtained explicit observational constraints on possible reflective compact objects whose surface radius r_s is close to the would-be event horizon radius r_h, $r_s = r_h(1 + \epsilon)$. According to [23], such objects with the "compactness parameter"

$1 + \epsilon < 1 + 10^{-3}$ are almost excluded.

In what follows we will discuss some simple examples of mirror star solutions to the 5D Einstein-Maxwell equations, which are special cases of static, spherically symmetric solutions obtained in [16,17]. Among them, the solution with a magnetic charge seems to be of largest interest, even though the smallness of extra dimensions, required for making them invisible by our instruments, leads to a severe restriction on mirror star masses, at least according to the solutions so far obtained. For comparison we also discuss the corresponding 5D black hole (BH) solutions, which also possess some features of interest.

We study their stability under spherically symmetric perturbations and determine the stability ranges of their parameters. According to our results, for stable mirror stars, the above-mentioned "compactness parameter" belongs to the range $1 + \epsilon \in (1, 2.002)$ (with a numerically obtained upper bound). Meanwhile, the black-hole solutions turn out to be stable in the whole range of their parameters, and we obtain estimates for the decay characteristics of their perturbations.

It should be noted that the objects that we call "magnetic mirror stars" have been recently discussed under the name of "topological stars" [24–26], and in [26] they were found to be stable under nonspherical perturbations. However, the stability range under spherically symmetric perturbations stated there does not coincide with ours, making necessary a further study. The methodologies of obtaining the solutions in question and their stability studies in [24–26] are different from ours, and therefore we believe that this comparison is of particular interest.

This paper is organized as follows. In Section 2 we consider the simplest example of a mirror-star solution being a 5D analogue of the Schwarzschild metric. Section 3 considers 5D Einstein-Maxwell fields, and it is concluded that among them the magnetic solutions of both black hole and mirror star types are of utmost interest. Their stability properties under spherically symmetric perturbations are studied in Section 4, and Section 5 is a conclusion.

2. Mirror Stars: A Simple Example

As mentioned above, in multidimensional space-times, in addition to BH solutions, there are families of so-called T-hole ones [16,17], formally obtained from BH ones by substituting $t \leftrightarrow v$, where v is one of the extra coordinates. However, they possess certain features connected with compactness of the extra dimensions, which are most clearly understood considering the simplest example on the basis of Schwarzschild's solution.

We will deal with 5D general relativity (GR) and static, spherically symmetric metrics of the form

$$ds_5^2 = \mathrm{e}^{2\gamma} dt^2 - \mathrm{e}^{2\alpha} du^2 - \mathrm{e}^{2\beta} d\Omega^2 + \eta_v \, \mathrm{e}^{2\xi} dv^2, \tag{1}$$

where u is the radial coordinate (admitting an arbitrary parametrization), v is the fifth coordinate, and $\eta_v = \pm 1$ depending on whether v is timelike $(+1)$ or spacelike (-1).

One of the vacuum solutions of this theory is the extended Schwarzschild solution, representing the Schwarzschild metric in its usual form with the added term $\eta_v dv^2$. The field equations "do not know" which of the coordinates is observable time and which is the extra one, hence there is another solution (to be called *T-Schwarzschild*) with the metric

$$ds_5^2 = dt^2 - \left(1 - \frac{2m}{r}\right)^{-1} dr^2 - r^2 d\Omega^2 + \left(1 - \frac{2m}{r}\right) \eta_v dv^2; \tag{2}$$

when crossing the value $r = 2m$, both signs of g_{rr} and g_{vv} simultaneously change. If $\eta_v = 1$, i.e., if the v direction is timelike at large r, the overall signature of the 5D metric is preserved, but in the opposite case, $\eta_v = -1$, it changes by four since two spacelike directions become timelike. Meanwhile, as can be directly verified, such a horizon is not a curvature singularity, both in the 5D metric and in its 4D section (The 4D part of (2), if we forget about the extra subspace, describes the so-called Schwarzschild traversable wormhole, in which $r = 2m$ is the throat).

If $\eta_v = 1$, the surface $r = 2m$ looks like a conventional Schwarzschild horizon in the (R, v) subspace, admitting an analytic extension from $r > 2m$ to $r < 2m$ with the corresponding Kruskal picture. However, if some points on the v axis are identified, as should be done to make the extra dimension small and invisible, then the corresponding wedge-like sectors are cut out in the Kruskal diagram, hence the T-region and R-region in the (r, v) subspace have only a single common point, i.e., the horizon intersection point, as shown in Figure 1. Instead of a horizon, we thus obtain a naked conical singularity at $r = 2m$.

Quite another picture is observed if $\eta_v = -1$. A joint study of the regions on different sides of the horizon might again be possible after a transition to coordinates in which the metric is manifestly nonsingular at $r = 2m$. Let us perform such a transition for (2) in a close vicinity of the would-be horizon $r = 2m$ bearing in mind that

other more complex cases can be treated in a similar manner:

$$r - 2m = \frac{x^2 + y^2}{8m}, \qquad v = 4m \arctan\Big(y/x\Big),$$
$$`ds_2^2(r, v) \approx \frac{r - 2m}{2m} dv^2 + \frac{2m}{r - 2m} dr^2 = dx^2 + dy^2. \tag{3}$$

Thus the (r, v) surface metric is locally flat near the location $r = 2m$, which is now transformed to the origin $x = y = 0$, while the v coordinate becomes a multiple of the polar angle.

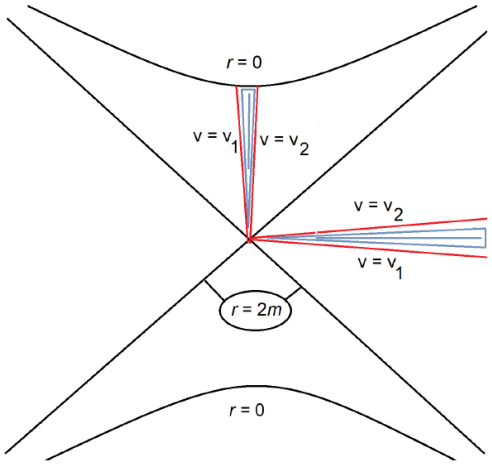

Figure 1. The Kruskal diagram for the metric (2) with a temporal extra dimension.

This transformation might be conducted as a conformal mapping of the complex plane with the analytic function $\log z, \;\; z = x + \mathrm{i}y$, then v is proportional to $\arg\, z$. Such an operation was performed in [27] for some special cylindrically symmetric Einstein-Maxwell solutions, see also [28].

As a result, in the general case, the (r, v) surface near $r = 2m$ behaves like a Riemann surface for the function $\log z$ that possesses a finite or infinite (if v varies in an infinite range) number of sheets, with its branching point located at $x = y = 0$, which can be called a branch-point singularity, following [27]. Furthermore, if the v direction is compact, then, since v now behaves as an angular coordinate, we can assume $0 \le v < 2\pi\ell$, where $v = 0$ and $v = 2\pi\ell$ are identified, and ℓ has the meaning of a compactification length in the asymptotic region ($r \to \infty$), where $g_{55} \to 1$. Thus $r = 2m$ is the center of symmetry in the (r, v) surface, and from (3) it follows that $r = 2m$ is a regular center under the condition $\ell = 2m$, it is an n-fold branch point if $l = 2m/n$, and at arbitrary ℓ there is a conical-type singularity. With a regular center, the (r, v) surface has the shape of a test tube that has a constant radius $\ell = 2m$ at large r, becomes narrower at smaller r and smoothly ends at $r = 2m$ (Figure 2).

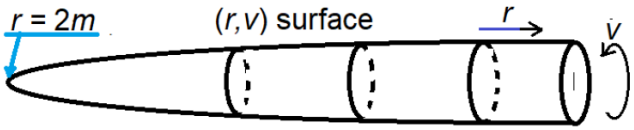

Figure 2. A regular $r-v$ surface in a T-Schwarzschild space-time with a spatial extra dimension.

It means that a radial geodesic, whose projection to the (r, v) surface hits the point $r = 2m$, passes through it and returns to larger values of r, though with another value of v, thus leaving a particular 4D section of space-time. However, if, instead of a classical point particle, we consider a quantum one, with a v-independent wave function, i.e., if it uniformly fills the v direction, then the particle certainly does not disappear from an observer's sight and can look as if reflected from a mirror. Such an assumption looks natural if the compactification length is sufficiently small, as should be the case in the framework of the Kaluza-Klein paradigm of extra dimensions. Possible v-dependent wave functions would belong to particles with extremely high energies corresponding to masses $\gtrsim 1/\ell$ in 4D.

We can conclude that this would-be horizon with $\eta_v = -1$ looks observationally like a mirror and can be called a *mirror surface*. However, as follows from the regularity condition $\ell = 2m$, such a mirror star has a very small mass: if we assume $\ell \sim 10^{-18}$ cm according to the instrumental constraints, we will obtain $m \sim 10^{15}\, m_{\rm Planck} \sim 10^{10}$ g,

a mass that, if it were a black hole, would evaporate via Hawking radiation in about one second. Quantum field effects close to a mirror surface can also be significant and deserve a separate study. Anyway, the direct relationship between this stellar mass and the compactification length is a challenge, and it is of great interest whether more complex models can if not avoid then at least weaken this constraint.

3. 5D Einstein-Maxwell Fields: Black Holes and Mirror Stars

As a next step, let us consider possible 5D analogs of the Reissner-Nordström solution of GR, introducing the Maxwell field with the Lagrangian $L = -F \equiv -F_{AB}F^{AB}$ as the only source of gravity with the static, spherically symmetric metric (1). It is clear that the solutions to be discussed are special cases of those considered in [16,17] and much more general multidimensional solutions of [5,29]; it nevertheless seems reasonable to discuss these simpler ones for better transparency of their expressions and properties.

Under the assumptions made, in addition to radial electric ($F_{01} = -F_{10}$) and magnetic ($F_{23} = -F_{32}$) fields, one more kind of electromagnetic field is compatible with the symmetry of (1), the one corresponding to the component $A_5(u)$ of the vector potential A_B, leading to nonzero components $F_{15} = -F_{51}$ of the electromagnetic tensor F_{AB}. Since such a component does not single out any direction in 3D space, it will be called "quasiscalar." The Maxwell equations

$$\partial_A\Big(\sqrt{|g|}F^{AB}\Big) = 0, \qquad \sqrt{|g|} = \mathrm{e}^{\alpha+2\beta+\gamma+\xi}\sin\theta, \tag{4}$$

for F^{01} and F^{15} depending on u only are easily solved with the corresponding charges as integration constants. For a magnetic field we have the usual expression corresponding to the potential component $A_3 = q_m\cos\theta$. As a result, it can be jointly written

$$\Big\{F_{01}F^{01},\ F_{23}F^{23},\ F_{15}F^{15}\Big\} = \Big\{-q_e^2\,\mathrm{e}^{-4\beta-2\xi},\ q_m^2\,\mathrm{e}^{-4\beta},\ -\eta_v q_s^2\,\mathrm{e}^{-4\beta-2\gamma}\Big\}, \tag{5}$$

where q_e, q_m, q_s are the electric, magnetic and quasiscalar charges, respectively.

Considering the existence of only one of the three kinds of electromagnetic fields, we can write the following expressions for their stress-energy tensors in all three cases:

$$\text{Electric}: \qquad T_A^B = q_e^2\,\mathrm{e}^{-4\beta-2\xi}\,\mathrm{diag}(1,1,-1,-1,-1), \tag{6}$$

$$\text{Magnetic}: \qquad T_A^B = q_m^2\,\mathrm{e}^{-4\beta}\,\mathrm{diag}(1,1,-1,-1,1), \tag{7}$$

$$\text{Quasiscalar}: \qquad T_A^B = \eta_v q_s^2\,\mathrm{e}^{-4\beta-2\gamma}\,\mathrm{diag}(-1,1,-1,-1,1). \tag{8}$$

One can notice that the energy density of a quasiscalar field is negative if the extra dimension is timelike.

The nonzero components of the Ricci tensor for the metric (1) can be written as follows without fixing the radial coordinate u (the prime denotes d/du):

$$\begin{aligned}
R_0^0 &= -\mathrm{e}^{-2\alpha}\Big[\gamma'' + \gamma'(2\beta' + \gamma' + \xi' - \alpha')\Big],\\
R_1^1 &= -\mathrm{e}^{-2\alpha}\Big[2\beta'' + \gamma'' + \xi'' + 2\beta'^2 + \gamma'^2 + \xi'^2 - \alpha'(2\beta' + \gamma' + \xi')\Big],\\
R_2^2 &= R_3^3 = \mathrm{e}^{-2\beta} - \mathrm{e}^{-2\alpha}\Big[\beta'' + \beta'(2\beta' + \gamma' + \xi' - \alpha')\Big],\\
R_5^5 &= -\mathrm{e}^{-2\alpha}\Big[\xi'' + \xi'(2\beta' + \gamma' + \xi' - \alpha')\Big],
\end{aligned} \tag{9}$$

where the coordinates are numbered as $(t, u, \theta, \varphi, v) = (0, 1, 2, 3, 5)$. Note that putting $\xi = \mathrm{const}$, we obtain the Ricci tensor components R_μ^ν of the 4D section of (1). It is also useful to present the Einstein tensor component $G_1^1 = R_1^1 - \frac{1}{2}R$ since the corresponding Einstein equation (the 5D Einstein equations have the form $G_B^A \equiv R_B^A - \frac{1}{2}R\delta_B^A = -T_B^A$) is first-order and is an integral of the others which are second-order:

$$G_1^1 = -\mathrm{e}^{-2\beta} + \mathrm{e}^{-2\alpha}\big(\beta'^2 + 2\beta'\gamma' + 2\beta'\xi' + \gamma'\xi'\big). \tag{10}$$

A further solution is best of all carried out using the harmonic radial coordinate u defined by the condition

$$\alpha = 2\beta + \gamma + \xi \tag{11}$$

in which case the Ricci tensor components take an especially simple form, as is evident in (9). Thus, the relation

$T_1^1 + T_2^2 = 0$, valid for all three kinds of electromagnetic fields, implies $R_0^0 + R_2^2 + R_5^5 = 0$, which in the coordinates (11) takes the form of the easily solved Liouville equation

$$\alpha'' - \beta'' = \mathrm{e}^{2\alpha - 2\beta} \quad \Rightarrow \quad \mathrm{e}^{\beta - \alpha} = s(k,u) \equiv \begin{cases} k^{-1} \sinh ku, & k > 0; \\ u, & k = 0; \\ k^{-1} \sin ku, & k < 0, \end{cases} \tag{12}$$

where $k = \mathrm{const} \in \mathbb{R}$, and one more integration constant is eliminated by choosing the zero point of u. Consequently, with no loss of generality, one can assert that the harmonic u coordinate is defined at $u > 0$, and $u = 0$ corresponds to spatial infinity.

The further solution looks differently for the three tensors (6), (7) and (8). In all three cases we will obtain the general solution and single out the cases containing horizon-like surfaces, which occur in the limit $u \to \infty$.

3.1. Electric Field

From different linear combinations of the Einstein equations it is easy to obtain

$$\xi'' + \frac{1}{2}\gamma'' = 0 \;\Rightarrow\; \xi = -\frac{1}{2}(\gamma + Nu) + \xi_0, \tag{13}$$

$$\gamma'' = Q^2 \mathrm{e}^{2\gamma} \quad \Rightarrow \quad \mathrm{e}^{2\gamma} = \frac{1}{Q^2 s^2(h, u + u_1)}, \tag{14}$$

where N, h, u_1, ξ_0 are integration constants, $Q = \sqrt{4/3} q_e$, and the function $s(h, u + u_1)$ is defined in the same way as in Equation (12). Two of the integration constants, u_1 and ξ_0, can be fixed by choosing the units along the t and v axes, in accord with asymptotic flatness at $u = 0$:

$$s^2(h, u_1) = Q^{-2}, \qquad \xi_0 = 0. \tag{15}$$

One more relation between the integration constants is obtained by substituting the expressions obtained to the Einstein equation $G_1^1 = -T_1^1$:

$$k^2 \operatorname{sign} k = \frac{3}{4} h^2 \operatorname{sign} h + \frac{1}{4} N^2. \tag{16}$$

Summarizing, we obtain the metric in the form

$$ds_5^2 = \mathrm{e}^{2\gamma} dt^2 - \frac{\mathrm{e}^{-\gamma + Nu}}{s^2(k,u)} \left[\frac{du^2}{s^2(k,u)} + d\Omega^2 \right] + \eta_v \, \mathrm{e}^{-\gamma - Nu} dv^2, \tag{17}$$

with e^{γ} presented in (14). The solution consists of a few branches with different analytical behaviors depending on the signs of the constants k and h.

It can be verified that a horizon within this solution is only possible in the case $h = k = N > 0$, and then the metric is presented in the most transparent form after the substitution $u \mapsto x$ such that

$$\begin{aligned} &\mathrm{e}^{-2ku} = 1 - \frac{2k}{x}, \qquad du = \frac{dx}{x^2(1 - 2k/x)}, \qquad \sinh ku = \frac{1 - k/x}{\sqrt{1 - 2k/x}}, \\ &\sinh[k(u + u_1] = \frac{k}{Q} \frac{1 + p/x}{\sqrt{1 - 2k/x}}, \qquad p = \sqrt{k^2 + Q^2} - k. \end{aligned} \tag{18}$$

This results in the black hole metric, asymptotically flat as $x \to \infty$,

$$ds_5^2 = \frac{1 - 2k/x}{(1 + p/x)^2} dt^2 - \left(1 + \frac{p}{x}\right) \left[\frac{dx^2}{1 - 2k/x} + x^2 d\Omega^2 - \eta_v dv^2 \right] \tag{19}$$

with an event horizon at $x = 2k$ and a singularity at $x = 0$. Unlike the Reissner-Nordström space-time, this one contains no Cauchy horizon, and the whole region $x < 2k$ has the nature of a Kantowski-Sachs cosmology that ends with a quasi-isotropic "big crunch" since both Kantowski-Sachs scale factors $\sqrt{|g_{00}|}$ and $\sqrt{|g_{22}|}$ behave at small x as $\sqrt{x}$, while the extra dimension blows up, $-g_{55} \sim 1/x$. The Carter-Penrose diagram for the (t, x) subspace is the same as for the Schwarzschild space-time.

3.2. Magnetic Field

Instead of (13) and (14), linear combinations of the Einstein equations now give

$$\mu'' = Q^2\, \mathrm{e}^{2\mu} \;\; \Rightarrow \;\; \mathrm{e}^{2\mu} = \frac{1}{Q^2 s^2(h, u+u_1)}, \;\; \text{where} \;\; \mu = \gamma + \xi, \tag{20}$$

$$\gamma'' = \xi'' \;\; \Rightarrow \;\; \gamma = \frac{1}{2}(\mu + Nu), \qquad \xi = \frac{1}{2}(\mu - Nu), \tag{21}$$

where N, h, u_1 are integration constants, now $Q = \sqrt{4/3}q_m$, and, as before, we have fixed the constants in such a way that $\gamma(0) = \xi(0) = 0$ in accord with asymptotic flatness at $u = 0$, and in particular, the relation (15) holds for $s(h, u_1)$. Also, as with the electric field, the Einstein equation $G^1_1 = -T^1_1$ leads to the relation (16) between the integration constants (note that the notations are chosen in a suitable way to obtain this similarity). The resulting metric has the form

$$ds_5^2 = \mathrm{e}^{\mu+Nu}dt^2 - \frac{\mathrm{e}^{-2\mu}}{s^2(k,u)}\left[\frac{du^2}{s^2(k,u)} + d\Omega^2\right] + \eta_v\, \mathrm{e}^{\mu-Nu}dv^2, \tag{22}$$

with e^{μ} presented in (20), and there are again a few branches of the solution depending on the signs of the constants k and h.

Metrics without naked singularities are obtained from (22) in the cases $k = h > 0$ and $N = \pm k$. Applying again the transformation (18), we obtain a black hole metric in the case $N = -k$,

$$ds^2_{5,\mathrm{bh}} = \frac{1-2k/x}{1+p/x}dt^2 - \left(1+\frac{p}{x}\right)^2\left[\frac{dx^2}{1-2k/x} + x^2 d\Omega^2\right] + \frac{\eta_v dv^2}{1+p/x}, \tag{23}$$

and a mirror star metric if $N = k$:

$$ds^2_{5,\mathrm{ms}} = \frac{dt^2}{1+p/x} - \left(1+\frac{p}{x}\right)^2\left[\frac{dx^2}{1-2k/x} + x^2 d\Omega^2\right] + \frac{1-2k/x}{1+p/x}\eta_v dv^2, \tag{24}$$

and they are related, as noted in the Introduction, by the replacement $dt^2 \rightleftarrows \eta_v dv^2$. The constants used here, $p > 0$ and $k > 0$, are related by

$$p = \sqrt{k^2 + Q^2} - k \;\; \Rightarrow \;\; k = \frac{4q^2 - 3p^2}{6p}, \tag{25}$$

where as before, $Q^2 = (4/3)q^2$. Each of these two metrics contains two independent physical parameters, for which one can choose the mass $m > 0$ and the charge $q = q_m$, and both metrics are conveniently rewritten in terms of the spherical radius $r = x + p$; however, they describe drastically different geometries, so let us discuss them separately.

Black holes:

with $r = x + p$, the metric (23) takes the form

$$ds^2_{5,\mathrm{bh}} = \frac{r-2m}{r}dt^2 - \frac{r^2 dr^2}{(r-2m)(r-p)} - r^2 d\Omega^2 + \frac{r-p}{r}\eta_v dv^2, \tag{26}$$

with the Schwarzschild mass $m = (p + 2k)/2$. Since $k > 0$, we have $p < 2m$, and with (25) it follows

$$3mp = 2q^2, \qquad q^2 < 3m^2. \tag{27}$$

This space-time contains an event horizon at $r = 2m > p$ and one more peculiar sphere $r = p > 0$, inside which the 4D metric acquires the Euclidean signature. Furthermore, if the extra coordinate v is temporal outside the object ($\eta_v = +1$), then the whole 5D metric becomes Euclidean at $r < p$ since all five coordinates become spatial, and the cosmological Kantowski-Sachs evolution terminates at $r = p$. Unlike that, if $\eta_v = -1$, then $r = p$ is a conventional Killing horizon in the (r, v) subspace. At $r \in (p, 2m)$, the only temporal coordinate is r, while at $r < p$ the only temporal coordinate is v. And this time variable is circular as long as $\{v\}$ is a circle. In all cases, $r = 0$ is a curvature singularity. What is important, in such black hole solutions the compactification length ℓ is not related to the mass m and charge q, and all these parameters are arbitrary (up to (27)).

Mirror stars:

from (24), in terms of $r = x + p$ we obtain

$$ds_5^2 = \frac{r-2m}{r}dt^2 - \frac{r^2dr^2}{(r-2m)(r-r_b)} - r^2d\Omega^2 + \frac{r-r_b}{r}\eta_v dv^2. \tag{28}$$

Here the Schwarzschild mass is $m = p/2$, but the sphere $r = 2m$, corresponding to the observable mass, is not an event horizon since a larger radius, $r_b = 2m + 2k$ is that of a mirror surface, which represents a boundary of this space-time as described above. Now, with (25), we obtain, instead of (27),

$$3mr_b = 2q^2, \qquad q^2 > 3m^2, \tag{29}$$

and at smaller q^2 this solution does not exist. In the metric (28), the expression of g_{tt} does not reach zero as r decreases: the solution terminates at larger r, so that a mirror star is less compact than a would-be black hole of the same mass.

A few words on the geodesic structure in this space-time. In any static, spherically symmetric space-time with the 4D part of the metric (1), 4D geodesics (those with $v = \mathrm{const}$) satisfy the equation (see, e.g., [30])

$$\mathrm{e}^{2\alpha+2\gamma}\left(\frac{du}{d\lambda}\right)^2 + V(u) = E^2, \qquad V(u) = \mathrm{e}^{2\gamma}(K + L^2/r^2), \qquad K = 0, \pm 1, \tag{30}$$

where u is an arbitrary radial coordinate, L and E are constants responsible for the conserved angular momentum and energy of a particle, λ is an affine parameter along timelike ($K = 1$), spacelike ($K = -1$) and null ($K = 0$) geodesics, respectively, and $V(u)$ is the effective potential, whose properties actually determine all features of the geodesic motion. Now, since $g_{00} = \mathrm{e}^{2\gamma}$ and $g_{22} = r^2$ in (28) are the same as in the Schwarzschild space-time, the 4D geodesic structure is also the same outside the boundary $r = r_b$. In particular, if $r_b < 3m$, then $r = 3m$ is an unstable photon sphere, while the boundary itself is a stable photon sphere.

If we require regularity of the metric at $r = r_b$, then a small size ℓ of the fifth dimension strongly restricts the solution parameters, similarly to Section 2:

$$4(m + k)^3 = k\ell^2. \tag{31}$$

The metric (28) coincides with the so-called "topological star" metric discussed in [24–26] under the identification

$$r_b = 2m + 2k \equiv r_B, \qquad r_{\mathrm{Scw}} = 2m \equiv r_S. \tag{32}$$

Thus r_B is the radius of the mirror sphere, while r_S is the Schwarzschild radius for the same mass.

Intermediate case: extremal black holes

At $q^2 = 3m^2$, that is, $p = 2m$ in (26), or equivalently $r_b = 2m$ in (28), we obtain the metric

$$ds_5^2 = \frac{r-2m}{r}dt^2 - \frac{r^2dr^2}{(r-2m)^2} - r^2d\Omega^2 + \frac{r-2m}{r}\eta_v dv^2. \tag{33}$$

That it describes an extremal black hole is made evident by using, for example, the new coordinate x defined by $r = 2m + x^2$, so that the metric reads

$$ds_5^2 = \frac{x^2}{(2m+x^2)^2}dt^2 - \frac{4(2m+x^2)^2dx^2}{x^2} - (2m+x^2)^2d\Omega^2 + \frac{x^2}{(2m+x^2)^2}\eta_v dv^2. \tag{34}$$

In this metric, $x \in \mathbb{R}$, and $x < 0$ describes a region beyond the horizon $x = 0$, with a geometry identical to $x > 0$. Curiously, in this case spherical radii smaller than $2m$ are impossible, and the whole system resembles a wormhole, but it is not traversable due to a horizon at its throat.

A separate solution may be obtained in the same manner for $r \le 2m$, but it seems to be of lesser interest and will not be discussed here.

3.3. Quasiscalar Fields

The results in this case are similar to those for an electric field with the substitutions $t \leftrightarrow v$ and $\gamma \leftrightarrow \xi$ but taking into account the two signs in $\eta_v = \pm 1$. Thus, instead of (13) and (14) we now obtain

$$\xi'' = \eta_v \, \mathrm{e}^{2\xi} \;\; \Rightarrow \;\; \mathrm{e}^{-2\xi} = \begin{cases} s^2(h, u + u_1), & \eta_v = +1, \\ h^{-2} \cosh^2[h(u + u_1)], \; h > 0, & \eta_v = -1, \end{cases} \tag{35}$$

$$\gamma'' + \frac{1}{2}\xi'' = 0 \;\; \Rightarrow \;\; \gamma = -\frac{1}{2}(\xi + Nu), \tag{36}$$

with integration constants N, h, u_1 and $Q = \sqrt{4/3} q_s$ and again adjusting to $\gamma(0) = \xi(0) = 0$. As before, Equation (16) is valid. The resulting metric has the form

$$ds_5^2 = \mathrm{e}^{-\xi - Nu} dt^2 - \frac{\mathrm{e}^{-\xi + Nu}}{s^2(k,u)} \left[\frac{du^2}{s^2(k,u)} + d\Omega^2 \right] + \eta_v \, \mathrm{e}^{2\xi} dv^2, \tag{37}$$

where e^{ξ} is given by (35), and there are even more branches of the solution with different k, h and η_v.

As before, solutions without naked singularities emerge in the case $k = h = N > 0$, which, after the substitution (18), leads to the metric

$$\begin{aligned} ds_5^2 &= \left(1 + \frac{p}{x}\right) \left[dt^2 - \frac{dx^2}{1 - 2k/x} - x^2 d\Omega^2 \right] + \eta_v \, \mathrm{e}^{2\xi} dv^2, \\ \mathrm{e}^{2\xi} &= \frac{1 - 2k/x}{(1 + p/x)^2}, \qquad \eta_v = 1, \\ \mathrm{e}^{2\xi} &= \frac{Q^2(1 - 2k/x)}{(k + p - kp/x)^2}, \qquad \eta_v = -1. \end{aligned} \tag{38}$$

As follows from the previous consideration, only in the case (38) this metric can correspond to a mirror star. Furthermore, as follows from the expression of g_{tt}, since $p > 0$, we hear deal with a negative Schwarzschild mass $m = -p/2$, therefore this metric does not seem to be physically relevant.

Thus, among the electrovacuum solutions, the magnetic solutions with the metrics (23) and (24) are of particular interest, and in what follows we will discuss their stability.

4. Magnetic Solutions: Reduction to 4D and the Stability Problem

4.1. General Consideration

Now we would like to determine the stability properties of the magnetic mirror star solution (24). While the solution itself was obtained directly in the 5D setting, a stability study turns out to be easier in the 4D setting using the Einstein conformal frame.

Thus, we are considering the 5D action with the matter Lagrangian L_m

$$S = \int d^5x \sqrt{{}^5g} ({}^5R + L_m) \tag{39}$$

in a manifold with the 5D metric

$$ds_5^2 = g_{\mu\nu} dx^\mu dx^\nu + \eta_v \, \mathrm{e}^{2\xi(x)} dv^2, \tag{40}$$

where, as before, $\eta_v = \pm 1$, the 4D metric $g_{\mu\nu}$ and the metric coefficient $g_{55} = \mathrm{e}^{2\xi(x)}$ do not depend on the 5th coordinate v. Then, integrating it out, we obtain, up to a constant factor and a full divergence,

$$S = \int d^4x \sqrt{{}^4g} \, \mathrm{e}^{\xi(x)} ({}^4R + L_m). \tag{41}$$

The next step is to transform it to the Einstein frame (E-frame) by the standard conformal mapping

$$g_{\mu\nu} \to \overline{g}_{\mu\nu} = \mathrm{e}^{\xi} g_{\mu\nu}, \tag{42}$$

which converts (41) to the form (again up to a full divergence)

$$S = \int d^4x \sqrt{^4\overline{g}} \Big({}^4\overline{R} + \frac{3}{2} \overline{g}^{\mu\nu} \xi_\mu \xi_\nu + e^{-\xi} L_m \Big), \tag{43}$$

where $\xi_\mu := \partial\xi/\partial x^\mu$, and the overbar marks quantities obtained from or with the metric $\overline{g}_{\mu\nu}$. Thus the 5D equations are reduced to 4D equations with a massless scalar field ξ minimally coupled to gravity but interacting with matter. The matter Lagrangian itself, in general, depends on the 5D metric, which is now reduced to the quantities $\overline{g}_{\mu\nu}$ and ξ. Since we are considering electrovacuum solutions, let us look how the electromagnetic invariant $\mathcal{F} = F_{AB}F^{AB}$ will appear in the action (43).

If there are only 4D components $F_{\mu\nu}$ while $F_{5\mu} = 0$, we have $\mathcal{F} = F_{AB}F^{AB} = F_{\mu\nu}F^{\mu\nu}$, and, since the expression $\sqrt{|g|}F_{\mu\nu}F^{\mu\nu}$ is invariant under conformal transformations, the same expression is valid in terms of the metric $\overline{g}_{\mu\nu}$. In particular, if $L_m = -\mathcal{F}$ (the 5D Maxwell Lagrangian), then Equation (43) takes the form well known as the action of dilaton gravity.

Unlike that, if $F_{5\mu} = \partial_\mu \chi \equiv \chi_\mu \neq 0$, where $\chi(x^\mu) = A_5$ is the extra-dimensional component of the vector potential (a quasiscalar field, see Sec. 3), we obtain $F_{5\mu}F^{5\mu} = \eta_v \, \mathrm{e}^{-2\xi} \overline{g}^{\mu\nu} \chi_\mu \chi_\nu$. Assuming that $F_{\mu\nu} = 0$ (that is, $F_{5\mu}$ are the only nonzero components of F_{AB}), we find

$$\mathcal{F} = F_{AB}F^{AB} = 2\eta_v \, \mathrm{e}^{-2\xi} \overline{g}^{\mu\nu} \chi_\mu \chi_\nu. \tag{44}$$

Thus we obtain an effective scalar field χ in 4D, this field is canonical if $\eta_v = -1$ (a spacelike extra dimension) and phantom if $\eta_v = 1$. As a result, in this case we have in 4D a special case of a sigma model with two interacting scalars ξ and χ, and its consideration is beyond the scope of this study.

So let us return to the action (43) with $L_m = -F_{\mu\nu}F^{\mu\nu}$ and write the E-frame metric in the form

$$\overline{ds}^2 = \mathrm{e}^{2\overline{\gamma}} dt^2 - \mathrm{e}^{2\overline{\alpha}} dx^2 - \mathrm{e}^{2\overline{\beta}} d\Omega^2, \tag{45}$$

where the barred notations $\overline{\alpha}, \overline{\beta}, \overline{\gamma}$ are similar to α, β, γ used in (1) but refer to our 4D E-frame metric.

For spherically symmetric perturbations of such models it is well known that they are determined by a single degree of freedom associated with the effective scalar field ξ of extra-dimensional origin, and since the action (43) is a special case of the action (A1) in [31] (with $\phi \mapsto \xi, h = 3/4, V = 0, S(\phi) \mapsto \mathrm{e}^{\xi}, q_e = 0$), we can actually use the perturbation equations obtained there. In this situation, the metric perturbations $\delta\overline{\alpha}, \delta\overline{\beta}, \delta\overline{\gamma}$ are also nonzero, but they only exist due to the spherically symmetric scalar perturbation $\delta\xi$, being connected via the Einstein equations.

Let us show this in more detail. Suppose that our equations due to (43) are solved for the static, time-independent variables $\xi, F_{\mu\nu}, \overline{\alpha}, \overline{\beta}, \overline{\gamma}$. Moreover, we are dealing with a magnetic solution, so that all $F_{\mu\nu}$ other than $F_{23} = -F_{32} = q \sin\theta$ are zero, and $F_{\mu\nu}F^{\mu\nu} = 2q^2 \, \mathrm{e}^{-4\overline{\beta}}$; note that this remains true in perturbed space-time. Then the scalar field equation for small time-dependent perturbations ("deltas") can be written as follows:

$$-\mathrm{e}^{2\overline{\alpha}-2\overline{\gamma}} \delta\ddot{\xi} + \delta\xi'' + (2\overline{\beta}' + \overline{\gamma}' - \overline{\alpha}')\delta\xi' + \xi'(2\delta\overline{\beta}' + \delta\overline{\gamma}' - \delta\overline{\alpha}') - \frac{2}{3} q^2 \delta\Big(\mathrm{e}^{2\overline{\alpha}-4\overline{\beta}+\xi} \Big) = 0, \tag{46}$$

where dots and primes denote $\partial/\partial t$ and $\partial/\partial x$, respectively, and the quantities $\xi, \overline{\alpha}, \overline{\beta}, \overline{\gamma}$ are taken from the static ("background") solution. Now, the Einstein equations make it possible to express the metric perturbations in terms of $\delta\xi$. In doing that, a necessary step is to fix the perturbation gauge, which means making a particular choice of a reference frame in perturbed space-time, and this is implemented by postulating some relation for the perturbations.

The relevant components of the Einstein equations (used in the form $R^\nu_\mu = -(T^\nu_\mu - \frac{1}{2}\delta^\nu_\mu T^\rho_\rho)$) are (tx) and $(\theta\theta)$. Without choosing a perturbation gauge they read, respectively,

$$2[\dot{\delta\overline{\beta}}' + \overline{\beta}'\dot{\delta\overline{\beta}} - \overline{\beta}'\dot{\delta\overline{\alpha}} - \overline{\gamma}'\dot{\delta\overline{\beta}}] = -\frac{3}{2}\xi'\dot{\delta\xi}, \tag{47}$$

$$\delta(\mathrm{e}^{-2\overline{\alpha}-2\overline{\beta}}) + \mathrm{e}^{2\overline{\alpha}-2\overline{\gamma}}\ddot{\delta\overline{\beta}} - \delta[\overline{\beta}'' + \overline{\beta}'(\overline{\gamma}' - \overline{\alpha}' + 2\overline{\beta}')] = q^2\delta\big(\mathrm{e}^{2\overline{\alpha}-4\overline{\beta}+\xi}\big). \tag{48}$$

It turns out that the gauge $\delta\overline{\beta} \equiv 0$ substantially simplifies the equations, so in what follows we employ this gauge. Then the (tx) component of the Einstein equations can be used to express $\delta\overline{\alpha}$ in terms of $\delta\xi$ and functions from the background solution:

$$2\overline{\beta}'\dot{\delta\overline{\alpha}} = \frac{3}{2}\xi'\dot{\delta\xi} \quad \Rightarrow \quad \delta\overline{\alpha} = \frac{3\xi'\delta\xi}{4\overline{\beta}'}. \tag{49}$$

Here, performing integration in t, we omit adding an arbitrary function of x since we are only interested in time-dependent perturbations. Next, the component $(\theta\theta)$ of the Einstein equations expresses the difference $\delta\overline{\alpha}' - \delta\overline{\gamma}'$ in terms of $\delta\overline{\alpha}$ and $\delta\xi$. Specifically,

$$\delta\overline{\gamma}' - \delta\overline{\alpha}' = \frac{1}{\beta'}\Big[\delta\Big(\mathrm{e}^{2\overline{\alpha}-2\overline{\beta}}\Big) - q^2\delta\Big(\mathrm{e}^{2\overline{\alpha}-4\overline{\beta}+\xi}\Big)\Big]. \tag{50}$$

Substituting (49) and (50) into the scalar wave equation (46), we exclude from it all metric perturbations, with the result

$$-\mathrm{e}^{2\overline{\alpha}-2\overline{\gamma}}\delta\ddot{\xi} + \delta\xi'' + (2\overline{\beta}' + \overline{\gamma}' - \overline{\alpha}')\delta\xi' - U(x)\delta\xi = 0, \tag{51}$$

where

$$U(x) = \mathrm{e}^{2\overline{\alpha}}\left[\frac{3\xi'^2}{2\overline{\beta}'^2}\Big(q^2\,\mathrm{e}^{\xi-4\overline{\beta}} - \mathrm{e}^{-2\overline{\beta}}\Big) + q^2\,\mathrm{e}^{\xi-4\overline{\beta}}\left(\frac{2\xi'}{\overline{\beta}'} + \frac{2}{3}\right)\right], \tag{52}$$

and, which is important, the choice of the radial coordinate is so far not fixed. Let us use this freedom, passing on to the "tortoise" coordinate z (such that $\overline{g}_{tt} = -\overline{g}_{zz}$), and also replace the unknown function, $\delta\xi \to \psi$, according to the relations

$$\frac{dx}{dz} = \mathrm{e}^{\overline{\gamma}-\overline{\alpha}}, \qquad \delta\xi(x,t) = \mathrm{e}^{-\overline{\beta}}\psi(x,t). \tag{53}$$

Then we arrive at the wave equation in its canonical form,

$$-\ddot{\psi} + \frac{d^2\psi}{dz^2} - V_{\mathrm{eff}}(z)\psi = 0, \tag{54}$$

with the effective potential

$$V_{\mathrm{eff}}(z) = \mathrm{e}^{2\overline{\gamma}-2\overline{\alpha}}\Big[U + \overline{\beta}'' + \overline{\beta}'(\overline{\beta}' + \overline{\gamma}' - \overline{\alpha}')\Big]. \tag{55}$$

The standard substitution $\psi(z) = \mathrm{e}^{i\omega t}Y(z)$ with some constant "frequency" ω converts (54) to the Schrödinger-like form

$$\frac{d^2Y}{dz^2} + \big[\omega^2 - V_{\mathrm{eff}}(z)\big]Y = 0. \tag{56}$$

Equation (56) with proper boundary conditions allows for a stability study, such that eigenvalues $\omega^2 \le 0$ correspond to perturbations growing with time.

It should be stressed that Equation (56) and, in particular, the potential V_{eff} are gauge-invariant, that is, are independent from the choice of a reference frame in perturbed space-time, and hence describe genuine physical perturbations. This invariance was explicitly proved in [32] by directly considering gauge transformations and is reflected in the fact that V_{eff} depends only on the functions characterizing the background solution.

We see that perturbations of the effective scalar field ξ of multidimensional origin determine all metric perturbations: specifically, in our gauge, $\delta\overline{\beta} = 0$, $\delta\overline{\alpha}$ is expressed in terms of $\delta\xi$ in Equation (49), and $\delta\overline{\gamma}'$ (using known $\delta\overline{\alpha}$) can be found from Equation (50); this determines $\delta\overline{\gamma}$ up to adding an arbitrary function of t that reflects arbitrariness of the time coordinate in a nonstatic space-time. In their turn, perturbations of the original 5D metric (1) are found in terms of $\delta\xi$ according to the transformation (42):

$$\delta\alpha = \delta\overline{\alpha} - \delta\xi/2, \qquad \delta\beta = -\delta\xi/2, \qquad \delta\gamma = \delta\overline{\gamma} - \delta\xi/2. \tag{57}$$

4.2. Spherical Perturbations of Magnetic Mirror Stars

As said above, this solution depends on two physical parameters, the mass m and the charge q, but it turns out to be more convenient to use, instead of q, the mirror horizon, or boundary, radius $r_b = 2q^2/(3m)$.

The scalar ξ and the components of the E-frame metric $\overline{g}_{\mu\nu}$ for the mirror star solution are given by

$$\mathrm{e}^{\xi(x)} = \frac{\sqrt{r-r_b}}{\sqrt{r}}, \qquad \mathrm{e}^{2\overline{\gamma}} = \mathrm{e}^{-2\overline{\alpha}} = \frac{(r-2m)\sqrt{r-r_b}}{r^{3/2}}, \qquad \mathrm{e}^{2\overline{\beta}} = \sqrt{r-r_b}\,r^{3/2}, \tag{58}$$

Accordingly, for the metric (58) we obtain

$$U(x) = -\frac{2r_b(3r_b-8m)}{(r-2m)(4r-3r_b)^2(r-r_b)}. \tag{59}$$

and the effective potential

$$V_{\rm eff}(x) = -\frac{r-2m}{16r^5(4r-3r_b)^2(r-r_b)}\Big[(512mr^4+128r^3(-13m+r)r_b \\ +16(152m-27r)r^2r_b^2+24r(-69m+16r)r_b^3+27(14m-3r)r_b^4)\Big], \tag{60}$$

its behavior is illustrated in Figure 3.

At large r and near the surface $r = r_b$, the potential (60) looks approximately as

$$V_{\rm eff}(x)\Big|_{r\to\infty} = \frac{4m+r_b}{2r^3}+O(r^{-4}), \qquad V_{\rm eff}(x)\Big|_{r\to r_b} = -\frac{(r_b-2m)^2}{16r_b^2(r-r_b)}+O(1). \tag{61}$$

The tortoise coordinate z, related to any x by (53) (now with $dx = dr$), has the asymptotic behavior

$$z \approx r \ \text{ as } \ r\to\infty, \qquad z \approx \frac{2r_b^{3/2}\sqrt{r-r_b}}{r_b-2m} \ \text{ as } \ r\to r_b, \tag{62}$$

assuming $z = 0$ at $r = r_b$ without loss of generality. Therefore, in terms of z,

$$V_{\rm eff}(z)\Big|_{z\to\infty} = \frac{4m+r_b}{2z^3}+O(z^{-4}), \qquad V_{\rm eff}(z)\Big|_{z\to 0} = -\frac{1}{4z^2}+O(1). \tag{63}$$

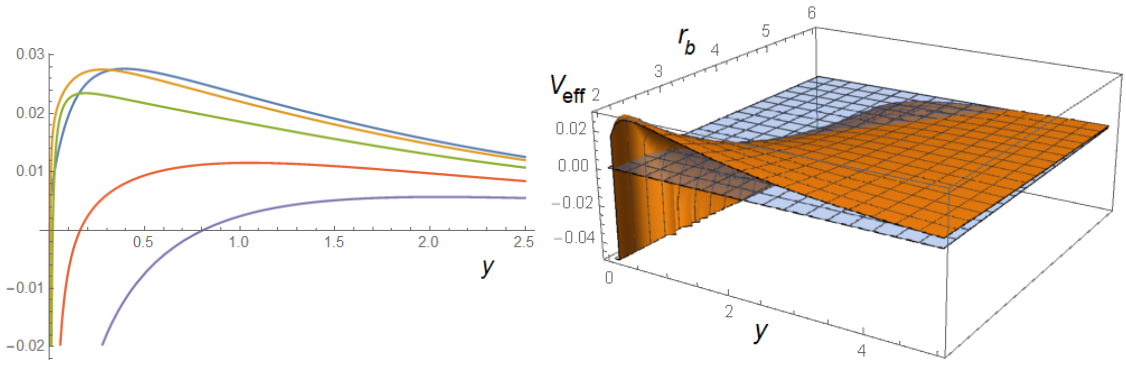

Figure 3. (**Left**): The effective potential $V_{\rm eff}$ for mirror star perturbations as a function of $y = r - r_b$ for $m = 1$ and $r_b - 2m = 0.02, 0.1, 0.3, 0.7, 1.3$ (upside-down at larger y). (**Right**): 3D plot of $V_{\rm eff}(y)$ for $m = 1$ and $r_b - 2m \in (0, 4)$. The transparent level $V_{\rm eff} = 0$ visualizes the region where $V_{\rm eff} > 0$. Note that the charge q is given by $q^2 = (3/2)mr_b$.

A study of the properties of $V_{\rm eff}$ allows for qualitative inferences. Thus, using (63), it is easy to obtain the asymptotic form of solutions to Equation (56) at large and small z for fixed $\omega^2 < 0$ (here and further on all $C_i = \text{const}$):

$$z\to\infty: \qquad Y(z) = C_1\,\mathrm{e}^{i\omega z}+C_2\,\mathrm{e}^{-i\omega z}, \tag{64}$$

$$z\to 0: \qquad Y(z) = \sqrt{z}(C_3+C_4\log z), \tag{65}$$

Now, let us discuss the boundary conditions. At large $z \approx r$, a natural requirement is a finite total energy of perturbations. The scalar field energy density is $\rho_\xi \sim \xi'^2$, so we have in the linear approximation $\delta\rho_\xi \sim \xi'\delta\xi'$, and since according to (58) $\xi' \sim 1/r^2$ at large r, for finiteness of the total energy we require $\rho_\xi = o(1/r^3)$, hence $\delta\xi' = o(1/r)$. On the other hand, if $\mathrm{Im}\,\omega \neq 0$, one of the terms in Equation (64) exponentially vanishes at large z while the other blows up, the latter being evidently incompatible with $\delta\xi' \sim (Y/r)' = o(1/r)$. Therefore, only the exponentially vanishing term is suitable, and our boundary condition for Y at large r must read simply $Y \to 0$.

Other subtle points must be discussed for the boundary $z = 0$. In similar cases, where $z = 0$ is a singularity and the effective potential behaves in the same way (see [33,34] among others), with the background scalar field $\xi \sim \log(r - r_b) \sim \log z$, and $Y \sim \psi \sim \delta\xi\sqrt{z}$, there seems to be no reason to require that $\delta\xi$ should blow up (if at all) slower than ξ itself. Then admitting $\delta\xi \sim \xi$ at small z, we obtain the boundary condition $Y \lesssim \sqrt{z}\log z$, so that all solution to Equation (56), with any finite ω, satisfy this condition. Hence physically admissible are perturbations growing in time with any increment $|\,\mathrm{Im}\,\omega|$, which means that the background configuration is catastrophically unstable, or, in other words, even small perturbations, having emerged, immediately show a nonlinear behavior.

However, in the present case, the value $z = 0$ corresponds to a regular surface in 5D space-time, and it is reasonable to require that perturbations preserve this regularity even though $g_{55} = -\,\mathrm{e}^{2\xi}$ vanishes there. It can be shown that the regularity requirement leads to $Y \lesssim \sqrt{z} \;\Rightarrow\; C_4 = 0$. This can be most easily verified using the trace of the 5D Einstein equation that gives

$$R = \frac{2}{3}T = \frac{2}{3}q^2\,\mathrm{e}^{-4\beta} = \frac{2}{3}q^2\,\mathrm{e}^{-4\overline{\beta}+2\xi} \tag{66}$$

(taking into account (57)). Since $\delta\overline{\beta} = 0$, a perturbation of the 5D curvature scalar R is simply $\delta R = 2R\delta\xi$ while $R(r_b) = \frac{2}{3}q^2 r_b^{-4} > 0$, and to keep R finite we must require $|\delta\xi| < \infty$. Recalling that $\delta\xi \sim Y/\sqrt{z}$ near $z = 0$ ($r = r_b$), we come to the condition $Y/\sqrt{z} < \infty$.

We conclude that our stability study requires solving a boundary-value problem for Equation (56) with the boundary conditions

$$Y \to 0 \;\text{ as }\; z \to \infty, \qquad Y/\sqrt{z} < \infty \;\text{ as }\; z \to 0. \tag{67}$$

It is then straightforward to show that the Schrödinger operator $-d^2/dz^2 + V_{\text{eff}}(z)$ with the boundary conditions (67) is self-adjoint in the Hilbert space of square-integrable functions $Y(z)$, which, according to the Sturm-Liouville theory, ensures that its spectrum is purely real, $\omega^2 \in \mathbb{R}$. Therefore, in our search for unstable modes of perturbations, we must seek solutions to Equation (56) with $\omega^2 < 0$, hence pure imaginary ω, and $Y(z) \sim \mathrm{e}^{-|\omega|z}$ as $z \to \infty$.

Let us stress that in the present approach we study perturbations emerging in our "isolated" system itself, rather than due to any signal or pumping coming from outside. This approach is, however, different from the one used in the analysis of quasinormal modes [4,35], where one requires that only outgoing waves are present, and one considers a field $\Phi \sim \mathrm{e}^{-i\omega(t-z)}$ at $\operatorname{Im}\omega < 0$ corresponding to a signal decreasing in time but growing at large z. Nevertheless, we can notice that in our case unstable perturbations growing exponentially in time and decaying at infinity also correspond to outgoing waves at large z.

Now, passing on to a numerical study, we have to take into account that the potential V_{eff} is expressed in terms of the coordinate r, connected with z by a transcendental equation, therefore, such a study is more conveniently conducted using Equation (51) written in terms of r. The substitution $\delta\xi(x) = \mathrm{e}^{i\omega t}X(x)$ (such that $X(r) = \mathrm{e}^{-\overline{\beta}}Y(z) \approx Y(z)/\sqrt{z}$) brings Equation (51) to the form

$$X'' + (2\overline{\beta}' + \overline{\gamma}' - \overline{\alpha}')X' + \left(\mathrm{e}^{2\overline{\alpha}-2\overline{\gamma}}\omega^2 - U(r)\right)X = 0, \tag{68}$$

and the boundary conditions (67) are equivalently rewritten as

$$X \underset{r\to\infty}{\longrightarrow} 0, \qquad |X(r_b)| < \infty. \tag{69}$$

4.3. Numerical Analysis for Magnetic Mirror Stars

An attempt to numerically solve Equation (68) by specifying the boundary condition at large r using Equation (64) with $C_1 = 0$ leads to a numerical instability near $r = r_b$. Therefore, let us try to use a "left to right" shooting procedure. A boundary precisely at $r = r_b$ cannot be specified as it is a singular point of the equation. So let us choose a boundary condition close to r_b, where a desired solution to Equation (68) should tend to a constant value. Suitable boundary conditions can be chosen by finding the asymptotic form of the solution $X(r)$ near $r = r_b$ in the next approximation to $X = X_0 = \text{const}$ (the assumed finite value at $r = r_b$).

For convenience, let us rewrite Equation (68) close to $r = r_b$ in terms of $y = r - r_b$. It reads

$$X'' + \frac{X'}{y} + \frac{K}{y}X = 0, \qquad K = \frac{r_b^3}{(r_b - 2m)^2}\omega^2 + \frac{6r_b - 16m}{r_b(r_b - 2m)}. \tag{70}$$

In general, it can be reduced to the Bessel equation, but we need its solution only close to $y = 0$ and seek it in the form $X = X_0 + cy^s,\ s > 0$. We find

$$s = 1, \qquad X = X_0(1 - Ky). \tag{71}$$

Therefore, a test function $X(y)$ in the shooting procedure with Equation (68) should satisfy the following boundary conditions at some small $y = y_0$:

$$X(y_0) = X_0(1 - Ky_0), \qquad X'(y_0) = -KX_0, \tag{72}$$

with K given in (70). The equation itself in terms of y has the form

$$X'' + \frac{2y + r_b - 2m}{y(y + r_b - 2m)} X' + \left[\frac{(y + r_b)^3}{y(y + r_b - 2m)^2} \omega^2 - U(y) \right] X = 0,$$
$$U = -\frac{2r_b(3r_b - 8m)}{y(y + r_b - 2m)(4y + r_b)^2} \tag{73}$$

The goal is to find such ω^2 that the solution $X(y)$ tends to zero as $y \to \infty$.

To implement the shooting method, we use the standard Runge-Kutta procedure for solving the Cauchy problem (70), (72), where y belongs to the interval $(y_0, y_1) \sim (10^{-3}, 10^3)$ giving the appropriate numerical accuracy for our purposes, and ω^2 is regarded as an unknown parameter varying inside some range $(\omega^2_{\min}, 0)$. For each test value of ω^2, we obtain the corresponding numerical curve $X_{\rm num}(y; \omega)$ satisfying the initial conditions (72). At the right end y_1, the value of $X_{\rm num}(y; \omega)$ strongly diverges if ω^2 does not coincide with an eigenvalue ω^2_0 of the differential operator (70), and becomes arbitrarily small as $\omega^2 \to \omega^2_0$ (recall that the latter means an instability of our static solution). Therefore, tracking the behavior of the curve $X_{\rm num}(y; \omega)$ at the right end allows us to reveal the stability and instability regions for various initial parameters of the system under consideration.

Without loss of generality, we put $m = 1$ and $X_0 = 1$, thus fixing the length scale for the problem and an insignificant factor in the solution for $X_{\rm num}$. Thus r_b remains the only nontrivial changeable parameter of the system.

The results of our numerical analysis are presented in Figure 4. The plot shows the existence of the eigenvalues ω^2 as functions of r_b and reveals the instability region at $r_b > r_b^{\rm crit}$, where $r_b^{\rm crit} \simeq 4.003996\, m$ is a critical value of r_b corresponding to the limiting case $\omega^2 = 0$. At $r_b < r_b^{\rm crit}$ the instability vanishes. The critical value $r_b^{\rm crit}$ can be easily found numerically from the condition of vanishing of the right-end value $X_{\rm num}(y_1)\big|_{\omega^2=0} \to 0$ as $r_b \to r_b^{\rm crit}$.

Figure 5 (left panel) shows examples of numerical curves $X_{\rm num}(y)$ for various ω^2 and r_b, and also a method for seeking the critical value $r_b^{\rm crit}$ (right panel).

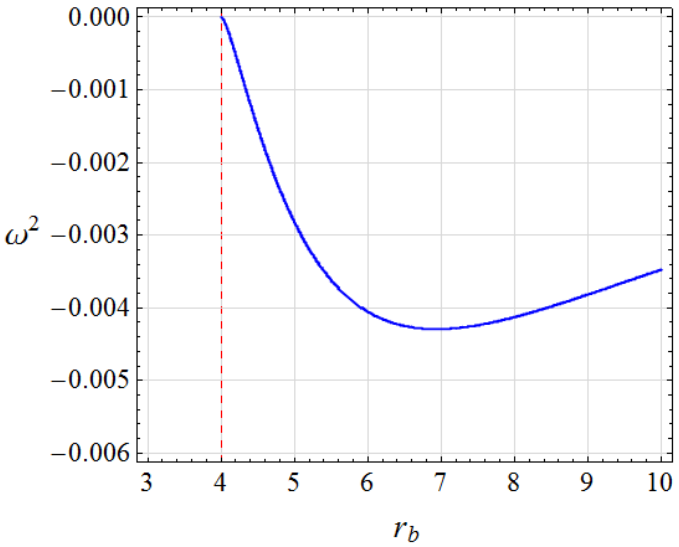

Figure 4. The eigenvalue ω^2 as a function of r_b. The red dashed line corresponds to $r_b = r_b^{\rm crit} \simeq 4.003996$, which shows the right boundary of the stability region.

The stability condition $r_b < r_b^{\rm crit}$ can also be rewritten in terms of m and q leading to a restriction on the ratio q^2/m^2. Combining it with the existence condition $q^2 > 3m^2$, we can finally write

$$1 < \frac{q^2}{3m^2} = \frac{r_b}{r_{\rm Scw}} \lesssim 2.001998. \tag{74}$$

Within this range, in accord with (25), the parameter k may be arbitrarily small, in other words, the mirror surface radius may be very close to the would-be Schwarzschild horizon. However, there is an observational constraint [23] on mirror surfaces according to which very small differences $\epsilon = r_b/r_{\rm Scw} - 1 \lesssim 10^{-3}$ look unlikely.

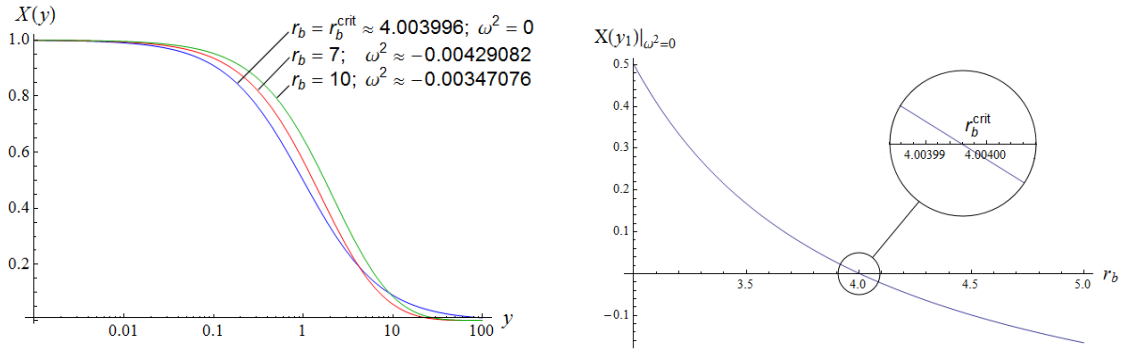

Figure 5. (**Left**): numerical curves $X_{\rm num}(y)$ for various ω^2 and r_b. (**Right**): vanishing of the right-end value $X_{\rm num}(y_1)\big|_{\omega^2=0}$ as a function of r_b allows us to find the critical value $r_b^{\rm crit} \simeq 4.003996$.

4.4. Spherical Perturbations of Magnetic Black Holes

For the black hole solution (26) we obtain the E-frame metric with

$$\mathrm{e}^{\xi(r)} = \frac{\sqrt{r-p}}{\sqrt{r}}, \qquad \mathrm{e}^{2\overline{\gamma}} = \mathrm{e}^{-2\overline{\alpha}} = \frac{(r-2m)\sqrt{r-p}}{r^{3/2}}, \qquad \mathrm{e}^{2\overline{\beta}} = r^{3/2}\sqrt{r-p}, \tag{75}$$

where $0 < p < 2m$. Hence the function U and the effective potential $V_{\rm eff}$ are

$$U(r) = \frac{2p(8m-3p)}{(4r-3p)^2(r-p)(r-2m)}, \tag{76}$$

$$V_{\rm eff}(r) = \frac{r-2m}{16(4r-3p)^2(r-p)r^5}\Big[378mp^4 - 9p^3(184m+9p)r + 128p^2(19m+3p)r^2 - 16p(104m+27p)r^3 + 128(4m+p)r^4\Big]. \tag{77}$$

The tortoise coordinate z is connected with r by the relations

$$z = \int \frac{r^{3/2}dr}{(r-2m)\sqrt{r-p}}, \qquad z\Big|_{r\to 2m} \approx \frac{\log(r-2m)}{\sqrt{m-p/2}}, \qquad r-2m\Big|_{z\to-\infty} \sim \exp\left[z\sqrt{m-p/2}\right]. \tag{78}$$

Thus $z \approx r$ at large r, and $z \to -\infty$ as $r \to 2m$. The asymptotic behavior of $V_{\rm eff}(r)$ is

$$V_{\rm eff}(r)\Big|_{r\to\infty} = \frac{4m+p}{r^3} + O(r^{-4}), \qquad V_{\rm eff}(r)\Big|_{r\to-\infty} \approx \exp\left[z\sqrt{m-p/2}\right]. \tag{79}$$

The asymptotic behavior of solutions to Equation (56) may be written as

$$Y(z) = C_5\,\mathrm{e}^{i\omega z} + C_6\,\mathrm{e}^{-i\omega z} \ \ (z\to\infty), \qquad Y(z) = C_7\,\mathrm{e}^{i\omega z} + C_8\,\mathrm{e}^{-i\omega z} \ \ (z\to-\infty). \tag{80}$$

At both infinities $V_{\rm eff}$ rapidly vanishes, and, as can be seen in Figure 6, it is positive at all $r > 2m$ for any p. Addressing the stability problem for such black holes in the above manner, similarly to mirror stars, we come to a boundary-value problem for Equation (56) with zero boundary conditions and seek eigenvalues $\omega^2 \in \mathbb{R}$. Then, the obtained $V_{\rm eff} > 0$ implies the absence of negative or zero eigenvalues ω^2, consequently, these black holes are stable under monopole perturbations at all values of $p \in (0, 2m)$.

This result makes natural our next step: find out how the black hole perturbations decay if allowed to lose their energy by radiating it either to infinity or to the horizon. This task can be solved by methods widely used in numerous studies of quasinormal modes. Though, here we should stress that quasinormal modes characterize "test" fields in the background of a fixed particular metric, while we are here considering the system's own perturbations of multidimensional origin, encompassing both scalar and metric disturbances.

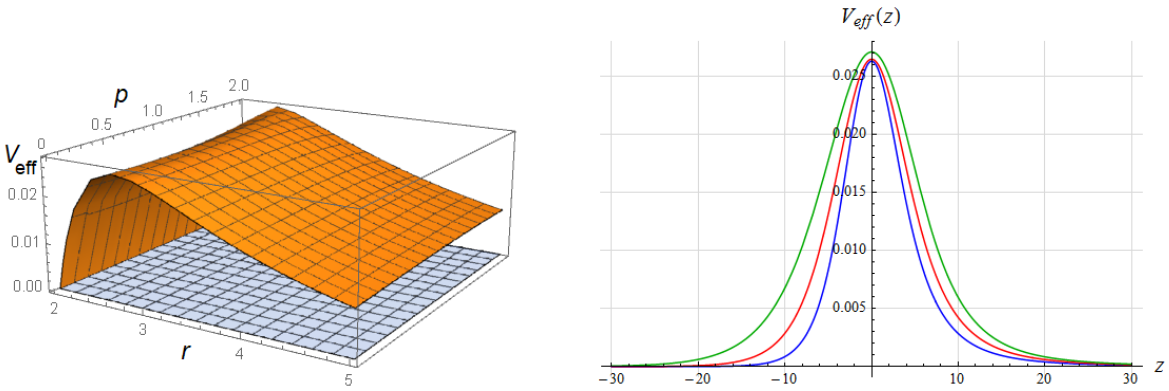

Figure 6. (**Left**): The effective potential for magnetic black hole perturbations (77) as a function of r and p. The transparent level $V_{\rm eff} = 0$ shows that $V_{\rm eff} > 0$ at all $r > 2m$. (**Right**): The effective potential as a function of z for $p = 0.1, 1, 1.5$ (bottom–up).

4.5. Black Hole Perturbation Dynamics

To determine the monopole perturbation spectrum under realistic conditions, we consider the wavelike Equation (54) with typical boundary conditions, corresponding to purely ingoing waves at the horizon and purely outgoing waves at spatial infinity. In terms of the tortoise coordinate, these conditions are expressed as

$$Y(z \to \pm\infty) \sim e^{\pm i\omega z}, \tag{81}$$

where ω is a generically complex quantity whose real part describes the oscillation frequency while the imaginary part accounts for the damping rate.

As can be seen from Figure 6, the effective potential $V_{\rm eff}(r)$ has a barrier with a single peak and smoothly decays at infinity and at the event horizon without any shape peculiarities. Such a good behavior of $V_{\rm eff}$ allows us to apply well-known numerical methods for calculation of the perturbations spectrum, widely used in the literature [4]. Here we use two of them: the WKB approach and the Time Domain Integration method.

The *WKB (Wentzel–Kramers–Brillouin) approach* is based on expansion of the solution to Equation (56) in the so-called WKB series near the event horizon and at infinity in accordance with the boundary conditions, and matching these asymptotic series with the Taylor expansion near the peak of the effective potential. This approach was originally developed by Will and Schutz [36] at the 1st WKB order and was extended to higher orders in the subsequent papers [37–39]. The general WKB formula for a frequency ω^2 can be written in the form [40]

$$\omega^2 = V_0 + A_2(\mathcal{K}^2) + A_4(\mathcal{K}^2) + ... - i\mathcal{K}^2\sqrt{-2V_2}(1 + A_3(\mathcal{K}^2) + A_5(\mathcal{K}^2) + ...), \tag{82}$$

where each k-th order correction term A_k is a cumbersome expression involving the values of higher-order derivatives of $V_{\rm eff}(z)$ at its maximum; here by V_0 and V_2 we denote the values of the effective potential and its second derivative at the maximum. There also exists an important improvement of the WKB method based on the Padé approximation technique [39,41], which in most cases significantly increases the accuracy.

While the WKB approach is generically applicable for "good" shapes of the effective potential, the convergence of the WKB series is asymptotic, i.e., it does not guarantee an increased accuracy at each subsequent order. Moreover, this method works much better in the case of higher multipole numbers $\ell \geq n$ (where n is an overtone number) and is generally not reliable in the case $\ell < n$. For $n = l$ the WKB method, especially improved by the Padé approximation, usually gives an acceptable accuracy that may be verified by comparison with other methods. We notice that the monopole perturbations under consideration correspond to $\ell = 0$, so we restrict ourselves to analyzing the fundamental mode $n = \ell = 0$ for different values of the parameter p (note that $p = 0$ corresponds to the Schwarzschild limit of the metric (75), and $p = 2$ to the extremal black hole (33), (34)).

In this particular study, we used the 9th order WKB method with $\tilde{m} = 4$, where $\tilde{m}$ is the polynomial degree in the corresponding Padé approximant expression [39,40]. This choice is not strictly necessary, and it is chosen to illustrate a good agreement with the results of another method based on time domain integration. Our analysis is not aimed at ultra-precise calculation of the spectrum, but rather at showing how typical approximate methods give a well-consistent result (within fractions of a percent), revealing a clear qualitative behavior of the system in the damped oscillatory regimes. For implementing the WKB procedure, we used the *Mathematica* algorithm publicly shared by the authors of [40].

To obtain the time evolution profile of perturbations at some fixed z (typically near the peak of the effective

potential), as well as to find the fundamental mode $n = 0$, one can use the so-called *Time Domain integration* (TD) method which is in fact direct numerical integration of the wavelike Equation (54) performed in the null-cone variables $u = t - z$, $v = t + z$ via the Gundlach-Price-Pullin discretization scheme [4,42]. In this method, the interior of the future light cone is discretized by a rhombic grid with a step h. Denoting the sides of a rhombic cell at the point (u, v) as $S = (u, v)$, $N = (u + h, v + h)$, $W = (u + h, v)$, $E = (u, v + h)$, the value of $\psi(N)$ can be calculated as

$$\psi(N) = \psi(W) + \psi(E) - \psi(S) - h^2 V_{\text{eff}}(S)\frac{\psi(W) + \psi(E)}{8} + \mathcal{O}(h^4). \tag{83}$$

This scheme allows for obtaining a discrete "time domain" profile $\psi(t)$ at a fixed point z for a given initial perturbation, typically chosen as a Gaussian wave package on the cone boundary [42]. The frequencies do not depend on the particular choice of this initial perturbation, thus an obtained TD profile can be used to extract the fundamental mode. For that, the Prony method is used [4] approximating the oscillatory part of a TD profile by a sum of terms $\sim C_j e^{-i\omega_j t}$ within an appropriate "fitting" range in t. In our case, the step $h = 0.025$ was used, and the fitting range is about from 20 to 70, which yields a reliable oscillatory profile and the parameters of the extracted fundamental mode.

The results of our analysis are presented in Table 1 and Figures 7 and 8, where all quantities are expressed in units corresponding to our choice $m = 1$. We see that the results obtained by the WKB-Pade and TD methods are in good agreement, mostly within the range of relative differences of a fraction of a percent (even though the case $n = \ell = 0$ is not the best for applicability of the WKB method), and provide a clear picture of the perturbations behavior with the changing parameter p. In particular, one can observe that the real part (oscillation frequency) grows as p increases, whereas the damping rate decreases, and the sensitivity of these quantities with respect to the change of p is roughly comparable. One can also easily check that the limiting case $p \to 0$ restores the Schwarzschild-type behavior of scalar perturbations. The other limiting case, the extremal black hole solution (33), (34) is also naturally included in the present setup.

The conclusion made above on the stability of the black hole solution under consideration is directly verified by the time domain integration performed for various values of the parameter $p \in (0, 2m)$, so that the corresponding TD profile always represents damped oscillations indicating the system stability under monopole perturbations.

Table 1. The fundamental mode $n = 0$ of black hole perturbations for various values of p calculated via the WKB Padé and TD methods, with the corresponding relative difference between them.

p	WKB9-Padé	TD	$\delta_{\text{Re},\%}$	$\delta_{\text{Im},\%}$
0.01	$0.111634 - 0.104343i$	$0.111504 - 0.104535i$	0.12	0.18
0.3	$0.117382 - 0.099482i$	$0.117460 - 0.099920i$	0.07	0.44
0.6	$0.123686 - 0.093657i$	$0.124024 - 0.094124i$	0.27	0.50
0.9	$0.131363 - 0.087391i$	$0.131315 - 0.087478i$	0.04	0.10
1.2	$0.138906 - 0.079178i$	$0.139222 - 0.079318i$	0.23	0.18
1.5	$0.147281 - 0.068716i$	$0.147572 - 0.068798i$	0.20	0.12
1.8	$0.154920 - 0.054365i$	$0.155696 - 0.054439i$	0.50	0.14
1.99	$0.162377 - 0.042098i$	$0.159158 - 0.042262i$	2.02	0.39

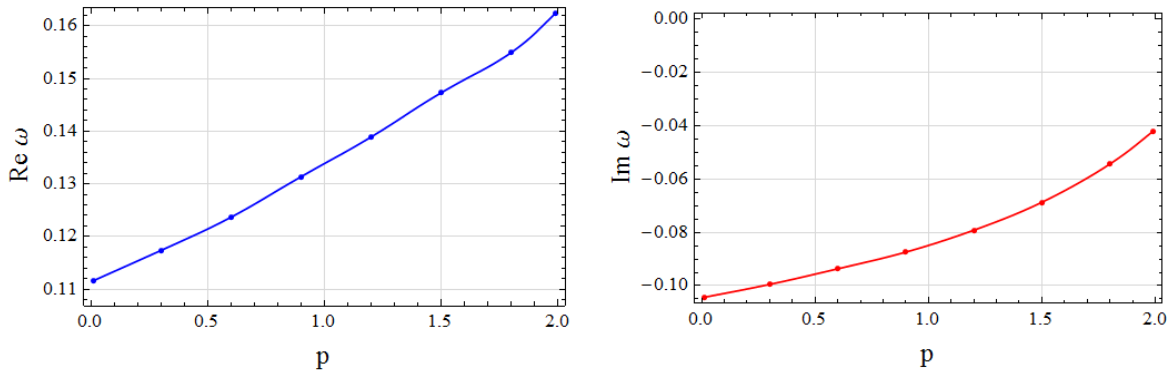

Figure 7. Graphic representations of the real and imaginary part of the WKB fundamental mode $n = 0$ interpolated between various values of p.

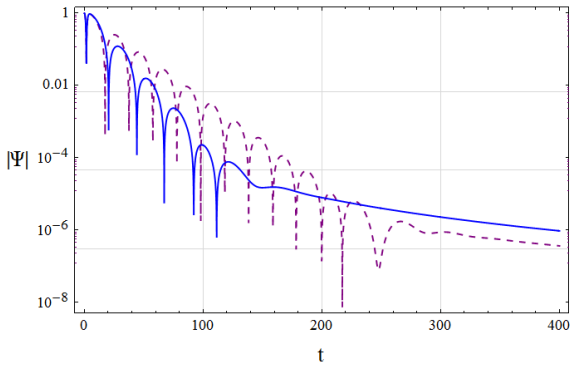

Figure 8. Example of the time domain profile for monopole perturbations with $p = 1$ (blue, solid) and $p = 1.8$ (purple, dashed).

5. Concluding Remarks

In this paper, we have determined the stability ranges of 5D magnetic mirror (topological) stars and black holes under linear monopole perturbations. For mirror stars, this stability range is given by Equation (74), that is, roughly, $1 < q^2/(3m^2) < 2$, while black holes turn out to be stable in the whole range $q^2/(3m^2) \leq 1$. At $q^2 > 6m^2$, mirror stars experience an instability due to evolution of the extra dimension whose metric coefficient g_{55} behaves as a 4D scalar field. These results evidently contradict some conclusions obtained by other authors. Thus, as asserted in [24], "topological stars are classically stable for the full range of parameters," while "magnetic black strings (i.e., black holes) are free from classical linear instability for $r_S/2 < r_B < r_S$," which in our notation means $1/2 < q^2/(3m^2) < 1$, contrary to our stability conclusion for all $q^2 \leq 3m^2$.

On the other hand, in [25,26], the range of the ratio $r_B/r_S = q^2/(3m^2)$ is divided into two sectors: Type I with $r_B/r_S > 3/2$, with a single photon sphere at $r = r_B$, and Type II ($1 < r_B/r_S \leq 3/2$) containing two photon spheres $r = 3m$ and $r = r_B$. In the introduction of [26], it is asserted that "the Type I sector was found to be free of instabilities," in contrast to our results: according to (74), the stability range covers the Type II sector but only partly the Type I sector. All these disagreements apparently require a further study.

For the black hole solutions under consideration, we have also studied the monopole perturbation dynamics, obtaining the spectrum of complex frequencies using the WKB and TD methods. The results demonstrate an agreement between these two methods and also well confirm our stability conclusions. For the stable range of mirror star models, a similar study cannot be carried out using the same standard methods which have to be modified owing to occurrence of a regular mirror surface instead of a horizon, and we postpone such a study for future work.

As follows from the regularity condition for mirror stars, their possible masses are related to the compactification length ℓ of the extra dimension and are therefore constrained to be lighter than $\sim 10^{10}$ g, see Section 2. Still one can notice that if we admit the multi-sheet nature of the extra dimension, then the regularity condition reads $\ell = 2m/n$, and at possible large n the mass m may be much larger than 10^{10} g. Note the corresponding discussion of "multiple bubbles" in [24]. More than that, if we forget the regularity requirement and admit a conical-type singularity (assuming that it must be somehow smoothed by quantum gravity effects), the restriction on m is no longer valid, while the mirror property for sufficiently light particles, in whose wave functions the length scale is much larger than ℓ, should be preserved. In addition, in any case, close to $r = 2m$ or $r = r_b$ we are dealing with strong gravitational fields and large curvatures, and it is necessary to consider QFT effects like those leading to Hawking black hole evaporation, which must be a subject of further studies.

Mirror stars of any size and mass and their possible clusters may be of interest from an observational viewpoint, in particular, as possible dark matter candidates. Even more interesting opportunities may emerge in the brane-world concept. For example, a particle may leave its brane with a certain probability and arrive at another brane.

Author Contributions

K.B.: conceptualization, methodology, writing—original draft preparation, visualization, writing—reviewing and editing; M.S.: writing—reviewing and editing, visualization, investigation; S.B.: writing—reviewing and editing, software, visualization, investigation. All authors have read and agreed to the published version of the manuscript.

Funding

This research received no external funding.

Institutional Review Board Statement

Not applicable.

Informed Consent Statement

Not applicable.

Data Availability Statement

Not applicable.

Conflicts of Interest

The authors declare no conflict of interest.

Use of AI and AI-Assisted Technologies

No AI tools were utilized for this paper.

References

1. Horowitz, G.T., (Ed.) *Black Holes in Higher Dimensions*; Cambridge University Press: Cambridge, UK, 2012.
2. Emparan, R.; Reall, H.S.; Black holes in higher dimensions. *Living Rev. Rel.* **2008**, *11*, 6.
3. Kanti, P. Black holes in theories with large extra dimensions: A review. *Int. J. Mod. Phys. A* **2004**, *19*, 4899–4951.
4. Konoplya, R.A.; Zhidenko, A. Quasinormal modes of black holes: from astrophysics to string theory. *Rev. Mod. Phys.* **2011**, *83*, 793.
5. Ivashchuk, V.D.; Melnikov, V.N. Exact solutions in multidimensional gravity with antisymmetric forms, *Class. Quantum Grav.* **2001**, *18*, R87–R152.
6. Torii, T.; Shinkai, Hi. Wormholes in higher dimensional space-time: Exact solutions and their linear stability analysis. *Phys. Rev. D* **2013**, *88*, 064027.
7. Deshpande, R.; Lunin, O. Charged wormholes in higher dimensions. *arXiv* **2022**, arXiv: 2212.11962v2.
8. DeBenedictis, A.; Das, A. Higher dimensional wormhole geometries with compact dimensions. *Nucl. Phys. B* **2003**, *653*, 279–304.
9. Baruah, A.; Deshamukhya, A. Traversable Lorentzian wormholes in higher dimensional theories of gravity. *J. Phys. Conf. Ser.* **2019**, *1330*, 012001.
10. Bronnikov, K.A.; Korolyov, P.A.; Makhmudov, A.; et al. Wormholes and black universes communicated with extra dimensions. *J. Phys. Conf. Ser.* **2017**, *798*, 012090.
11. Hartmann, B.; Kleihaus, B.; Kunz, J.; et al. Rotating boson stars in 5 dimensions. *Phys. Rev. D* **2010**, *82*, 084022.
12. Brihaye, Y.; Delsate, T. Boson stars, neutron stars and black holes in five dimensions. *arXiv* **2016**, arXiv:1607.07488.
13. Franzin, E. Mini boson stars in higher dimensions are radially unstable. *Gen. Rel. Grav.* **2024**, *56*, 107.
14. Ghosh, S.; Rahaman, F.; Guha, B.K.; et al. Charged gravastars in higher dimensions, *Phys. Lett. B* **2017**, *767*, 380.
15. Latief, A.O.; Akbar, F.T.; Gunara, B.E. Effective spacetime geometry of graviton condensates in f(R) gravity. *Phys. Rev. D* **2020**, *102*, 024036.
16. Bronnikov, K.A. Spherically symmetric solutions in D-dimensional dilaton gravity. *Grav. Cosmol.* **1995**, *1*, 67–78.
17. Bronnikov, K.A. Extra dimensions and possible space-time signature changes. *Int. J. Mod. Phys. D* **1995**, *4*, 491–516.
18. Bronnikov, K.A.; Bolokhov, S.V.; Skvortsova, M.V. Magnetic mirror stars in five dinensions. *Grav. Cosmol.* **2025**, *31*, 166.
19. Biswas, S.; Singha, C.; Chakraborty, S. Galactic wormholes: Geometry, stability, and echoes. *arXiv* **2023**, arXiv:2307.04836.
20. Bronnikov, K.A.; Konoplya, R.A. Echoes in brane worlds: Ringing at a black hole-wormhole transition. *Phys. Rev. D* **2020**, *101*, 064004.
21. Rosato, R.F.; Biswas, S.; Chakraborty, S.; et al. Greybody factors, reflectionless scattering modes, and echoes of ultracompact horizonless objects. *arXiv* **2025**, arXiv:2501.16433.
22. Uchikata, N.; Narikawa, T.; Nakano, H.; et al. Searching for gravitational wave echoes from black hole binary events in the third observing run of LIGO, Virgo, and KAGRA collaborations. *arXiv* **2023**, arXiv:2309.01894.
23. Mastrogiovanni, S.; Maggio, E.; Mascioli, A.F. Limits on the existence of totally reflective exotic compact objects with current and future gravitational-wave detectors. *arXiv* **2025**, arXiv:2502.07675.
24. Bah, I.; Heidmann, P. Topological stars and black holes, *Phys. Rev. Lett.* **2021**, *126*, 151101.
25. Dima, A.; Melis, M.; Pani, P. Spectroscopy of magnetized black holes and topological stars, *Phys. Rev. D* **2024**, *110*, 084067.
26. Dima, A.; Melis, M.; Pani, P. Nonradial stability of topological stars. *arXiv* **2025**, arXiv: 2502.04444.
27. Bronnikov, K.A. Inverted black holes and anisotropic collapse. *Russ. Phys. J.* **1979**, *22*, 594–600.

28. Bronnikov, K.A.; Santos, N.; Wang, A. Cylindrical systems in general relativity (review). *Class. Quantum Grav.* **2020**, *37*, 113002.
29. Bronnikov, K.A.; Ivashchuk, V.D.; Melnikov, V.N. The Reissner-Nordström problem for intersecting electric and magnetic p-branes. *Grav. Cosmol.* **1997**, *3*, 203–212.
30. Bronnikov, K.A.; Rubin, S.G. *Black Holes, Cosmology and Extra Dimensions*; World Scientific: Singapore, 2022.
31. Bronnikov, K.A.; Korolyov, P.A. Magnetic wormholes and black universes with invisible ghosts. *Grav. Cosmol.* **2015**, *21*, 157–165.
32. Bronnikov, K.A.; Fabris, J.C.; Zhidenko, A. On the stability of scalar-vacuum space-times. *Eur. Phys. J. C* **2011**, *71*, 1791.
33. Bronnikov, K.A.; Khodunov, A.V. Scalar field and gravitational instability. *Gen. Rel. Grav.* **1979**, *11*, 13.
34. Bronnikov, K.A.; Bolokhov, S.V.; Skvortsova, M.V.; et al. On the stability of spherically symmetric space-times in scalar-tensor gravity. *Grav. Cosmol.* **2023**, *29*, 374–386.
35. Berti, E.; Cardoso, V.; Starinets, A.O. Quasinormal modes of black holes and black branes. *Class. Quantum Grav.* **2009**, *26*, 163001.
36. Schutz, B.F.; Will, C.M. Black hole normal modes: A semianalytic approach. *Astrophys. J. Lett.* **1985**, *291*, L33.
37. Iyer, S.; Will, C.M. Black hole normal modes: A WKB approach. 1. Foundations and application of a higher order WKB analysis of potential barrier scattering. *Phys. Rev. D* **1987**, *35*, 3621.
38. Konoplya, R.A. Quasinormal behavior of the d-dimensional Schwarzschild black hole and higher order WKB approach. *Phys. Rev. D* **2003**, *68*, 024018.
39. Matyjasek, J.; Opala, M. Quasinormal modes of black holes. The improved semianalytic approach. *Phys. Rev. D* **2017**, *96*, 024011.
40. Konoplya, R.A.; Zhidenko, A.; Zinhailo, A.F. Higher order WKB formula for quasinormal modes and grey-body factors: Recipes for quick and accurate calculations. *Class. Quantum Grav.* **2019**, *36*, 155002.
41. Hatsuda, Y. Quasinormal modes of black holes and Borel summation. *Phys. Rev. D* **2020**, *101*, 024008.
42. Gundlach, C.; Price, R.H.; Pullin, J. Late time behavior of stellar collapse and explosions: 1. Linearized perturbations. *Phys. Rev. D* **1994**, *49*, 883.